NMR Mapping of the Recombinant Mouse Major Urinary Protein I Binding Site Occupied by the Pheromone 2-*sec*-Butyl-4,5-dihydrothiazole†

Lukáš Žídek, Martin J. Stone,* Susan M. Lato, Mark D. Pagel, Zhongshan Miao, Andrew D. Ellington, and Milos V. Novotny*

Department of Chemistry, Indiana University, Bloomington, Indiana 47405

Received March 2, 1999; Revised Manuscript Received June 1, 1999

ABSTRACT: The interactions between the mouse major urinary protein isoform MUP-I and the pheromone 2-*sec*-butyl-4,5-dihydrothiazole have been characterized in solution. ^{15}N-labeled and ^{15}N,^{13}C-doubly-labeled recombinant MUP-I were produced in a bacterial expression system and purified to homogeneity. Racemic 2-*sec*-butyl-4,5-dihydrothiazole was produced synthetically. An equilibrium diffusion assay and NMR titration revealed that both enantiomers of the pheromone bind to the recombinant protein with a stoichiometry of 1 equiv of protein to 1 equiv of racemic pheromone. A micromolar dissociation constant and slow-exchange regime dissociation kinetics were determined for the pheromone−protein complex. ^{1}H, ^{15}N, and ^{13}C chemical shifts of MUP-I were assigned using triple resonance and ^{15}N-correlated 3D NMR experiments. Changes in protein $^{1}H^{N}$ and $^{15}N^{H}$ chemical shifts upon addition of pheromone were used to identify the ligand binding site. Several amide signals, corresponding to residues on one side of the binding site, were split into two peaks in the saturated protein−ligand complex. Similarly, two overlapping ligand spin systems were present in isotope-filtered NMR spectra of labeled protein bound to unlabeled pheromone. The two sets of peaks were attributed to the two possible chiralities of the pheromone. Intermolecular NOEs indicated that the orientation of the pheromone in the MUP-I binding cavity is opposite to that modeled in a previous X-ray structure.

The urine of male mice contains unusually high concentrations of protein (*1*). Most urinary proteins belong to a group of closely related polypeptides, collectively referred to as the major urinary protein (MUP).[1] MUP genetics have been studied extensively, and several dozen MUP genes have been identified and classified (*2*−*6*). On the basis of nucleic acid sequence, the MUP genes have been classified into groups (*2*). Most MUPs are products of group 1 genes (*2*). They are expressed in the liver under multiple hormone control (*6, 7*) and excreted into the urine. Other tissues, including mammary, parotid, sublingual, submaxillary, and lachrymal glands, produce highly homologous proteins which are often designated as MUP isoforms (*8, 9*). The expression of MUPs is strongly sex-specific. Although most of the proteins are produced by males, some MUPs are expressed by females (*8, 10*). Dependence of the expression patterns on the strain has been monitored mass-spectrometrically (*11*). Common inbred strains seem to belong to one of two expression classes (*12*), while the wild mouse populations exhibit higher heterogeneity (*13*).

Although the exact biological function of MUPs is not well understood at present, they are believed to play a role in pheromonal communication in the mouse (*14, 15*). Numerous mouse pheromones have been isolated from the urine and other sources and prepared synthetically (*16*). The laboratory-made substances promote inter-male aggression (*17*), estrus synchronization (*18*), and puberty inhibition in females (*19*). Two of these pheromones, 2-*sec*-butyl-4,5-dihydrothiazole (structure 1) and 3,4-dehydro-*exo*-brevicomin, were found to coelute with the MUP fraction during size-exclusion chromatography of the male mouse urine (*20*). Dissociation constants measured for complexes of these pheromones with MUPs were approximately 10 μM (*21*). It has been postulated that MUPs may act as slow releasers of the pheromones which would otherwise disappear quickly from the environment due to their volatility (*15*).

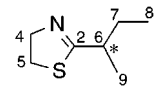

structure 1

The 2.4 Å resolution crystal structure of a MUP isolated from mouse urine (*14*) revealed that MUPs can be classified as lipocalins, i.e., small, extracellular proteins able to bind hydrophobic ligands. MUP polypeptide chain (molecular

† This work was supported by Grants DC 02418 (to M.V.N.) and GM 55055 (to M.J.S.) from the National Institutes of Health, and by Grant MCB-9600968 (to M.J.S.) from the National Science Foundation.

* Address correspondence to these authors. M.V.N.: Phone: 812-855-4532. Fax: 812-855-8300. Email: novotny@indiana.edu. M.J.S.: Phone: 812-855-6779. Fax: 812-855-8300. Email: mastone@indiana.edu.

[1] Abbreviations: MUP, major urinary protein; rMUP-I, recombinant MUP-I; DNA, deoxyribonucleic acid; SDS, sodium dodecyl sulfate; DSS, 3-(trimethylsilyl)-1-propanesulfonic acid, sodium salt; Tris, tris-(hydroxymethyl)aminomethane; PAGE, polyacrylamide gel electrophoresis; MALDI-TOF-MS, matrix-assisted laser desorption/ionization time-of-flight mass spectrometry; NMR, nuclear magnetic resonance; HSQC, heteronuclear single-quantum coherence; NOE, nuclear Overhauser effect; NOESY, nuclear Overhauser effect spectroscopy; TOCSY, total correlation spectroscopy. The acronyms of NMR experiments not listed above are based on symbols of nuclei. The order of nuclei symbols indicates magnetization transfer, and parentheses indicate nuclei not subjected to chemical shift evolution in three-dimensional experiments.

10.1021/bi990497t CCC: $18.00
Published on Web 07/16/1999

mass of ~19 000 Da) is folded into a characteristic barrel formed by eight antiparallel β-strands designated A−H (*22*). One end of the barrel is capped with a short N-terminal 3_{10}-helix. The C-terminal region and a loop connecting strands A and B together close the other end of the barrel where a ligand has been proposed to enter a hydrophobic binding cavity (*22*). In the crystal structure, the cavity contained diffuse electron density attributed to a bound pheromone modeled as (*S*)-2-*sec*-butyl-4,5-dihydrothiazole. However, given the possible heterogeneity of both the protein and ligand in the crystal sample, the precise identity and nature of the protein−ligand interactions remain poorly defined. To date it has been difficult to obtain homogeneous authentic MUP protein in sufficient quantites for structural studies. The material from mammalian sources is heterogeneous, and the reported MUP-II isoform expressed in *Pichia pastoris* contains an unidentifed covalent modification (*23*).

The goal of the present study was to characterize the interactions of the urinary protein isoform MUP-I with the natural pheromonal ligand, 2-*sec*-butyl-4,5-dihydrothiazole, using highly homogeneous samples of both protein and ligand. We used an *Escherichia coli* expression system to obtain high yields of MUP-I, while 2-*sec*-butyl-4,5-dihydrothiazole was prepared synthetically. The recombinant protein binds the synthetic pheromone with micromolar affinity. The protein was labeled biosynthetically with ^{15}N and ^{13}C, and the NMR resonances and secondary structure of the protein were assigned. The pheromone binding site, stoichiometry, and ligand orientation were detemined by NMR analysis.

MATERIALS AND METHODS

Materials. Electrophoretic reagents were purchased from Bio-Rad Laboratories (Richmond, CA). Buffers for liquid chromatography and NMR spectroscopy were obtained from Fluka (Ronkonkoma, NY). Deionized distilled water and 99.9% deuterium oxide (Cambridge Isotope Laboratories, Andover, MA) were used as solvents. 2-*sec*-Butyl-4,5-dihydrothiazole was synthesized as described previously (*24*). 2-Isobutyl-4,5-dihydrothiazole was prepared through a reaction of 2-aminoethanethiol with ethyl-1-imino-2-methylbutyl ether (*25*). New England Biolabs (Beverly, MA) enzymes, Qiagen columns (Chatsworth, CA), and Novagen (Madison, WI) and Invitrogen (San Diego, CA) reagents and plasmids were used for cloning. DNA was synthesized and sequenced at the departmental facility with Perkin-Elmer (San Jose, CA) chemicals and equipment (ABI 391 DNA Synthesizer and ABI PRISM 377 DNA Sequencer). Factor Xa protease was a product of Promega (Madison, WI). Other chemicals were products of Sigma (St. Louis, MO) of the highest available quality.

Construction of the Expression Vector. cLiv1 clone (*8*), containing the MUP-I gene, inserted into pTZ18R plasmid was a gift from Dr. J. Bishop (Centre for Genome Research, The University of Edinburgh, U.K.). The mature protein-encoding sequence of MUP-I was amplified by polymerase chain reaction using the following primers. The 5′ primer 5′-GCAATA**CC ATG G**GC CAT CAT CAT CAT CAT CAT AGC AGC GGC CAT ATCGAAGGTCGT *GAA GAA GCT AGT TCT ACG*-3′ introduced an *Nco*I restriction site (bold) and a hexahistidine tag coding sequence (singly underlined) terminated by a factor Xa protease recognition site (doubly underlined) immediately preceding the sequence encoding the N-terminus of the mature MUP-I protein (italics). The 3′ primer 5′-GACG**CTCGAG** *TCA TTC TCG GGC CTG GAG*-3′ contained an *Xho*I restriction site (bold) and a sequence complementary to the C-terminus with the TGA stop-codon (italics). The amplified fragment was inserted into a pCR-Blunt vector (Invitrogen) and digested with *Nco*I and *Xho*I, consecutively. The insert was purified and ligated between the *Nco*I and *Xho*I restriction sites of pET-28b(+) plasmid (Novagen). *E. coli* DH5α cells (Invitrogen) were used for cloning. The recombinant plasmid was transformed into *E. coli* BL21(DE3) for protein expression.

Protein Expression and Purification. One liter of M-9 minimal medium (containing 6 g of Na_2HPO_4, 3 g of KH_2PO_4, 0.5 g of NaCl, 1 g of NH_4Cl, 2 g of glucose, 0.24 g of $MgSO_4$, 14.7 mg of $CaCl_2 \cdot 2H_2O$, and 50 mg of kanamycin) was inoculated with an overnight culture from a single colony of the BL21(DE3) transformant and incubated, with shaking at 37 °C. When the absorbance at 600 nm reached 0.6, expression was induced by addition of 10 mL of 0.1 M isopropyl-β-thiogalactopyranoside. After an additional 18 h, the cells were harvested by centrifugation (10 min at 5000*g*). The cell pellet was resuspended in 20 mL of binding buffer (5 mM imidazole, 500 mM sodium chloride, 20 mM Tris-HCl, pH 7.9), and the cells were lysed by three freeze−thaw cycles followed by sonication for 6 min. The lysate was centrifuged at 30000*g* for 40 min. The supernatant was filtered and loaded onto a column containing 5 mL of Novagen His-Bind resin and washed with 50 mL of binding buffer. The hexahistidine-tagged protein was eluted with binding buffer containing 0.2 M imidazole, desalted, and concentrated in Amicon Microcon 10 centrifugal microconcentrators. The buffer was exchanged into 100 mM sodium chloride, 1 mM calcium chloride, 50 mM Tris-HCl, pH 7.9, during concentration. The tag was cleaved off with 100 μg (approximately 12 units) of factor Xa protease per 0.7 mL of solution containing approximately 20 mg of the protein. After 2.5 days of incubation at 21 °C, rMUP-I was purified by anion-exchange chromatography on a Pharmacia Source 15Q HR 5/5 column (at a flow rate of 0.5 mL/min of 10 mM Tris-HCl, pH 7.9, gradient of 0−0.5 M sodium chloride in 30 min). ^{15}N-Labeled ammonium chloride (1 g/L) and [^{13}C]glucose (2 g/L) were used to prepare isotopically labeled protein samples (*26*).

Protein Characterization. Protein expression was monitored by SDS−PAGE. Isoelectric focusing was performed in T3C5 polyacrylamide gels with 1.6% Biolyte 4/6 and 0.4% Biolyte 3/10 using a Bio-Rad Bio-Phoresis horizontal cell. Anion-exchange chromatography was performed on a Pharmacia Smart System equipped with a MiniQ PC 3.2/3 column (Pharmacia, Piscataway, NJ). Matrix-assisted laser desorption ionization time-of-flight mass spectrometry was performed on a Perseptive Biosystems (Framingham, MA) Voyager RPDE Biospectrometry Workstation, in a delayed-extraction mode using sinapinic acid as a sample matrix.

Binding Assays. The dissociation constant of rMUP-I/2-*sec*-butyl-4,5-dihydrothiazole complex was determined using the method of Ferrari et al. (*23*), followed by gas chromatography of the pheromone. Fifty microliter protein-containing drops were placed above a 15 mL reservoir with a solution of varying ligand concentration in the same buffer

(10 mM sodium phosphate, pH 6.3). After a 36 h incubation at 21 °C, the drops were extracted with an equal volume of *n*-heptane. Six microliters of the organic extract was mixed with 3 μL of internal standard (10 μg/mL indole in *n*-heptane) and injected into a gas chromatographic capillary column (SE-54, 0.25 mm internal diameter, 30 m length, and 0.25 μm film thickness). The chromatographic analyses were performed with a Hewlett-Packard (Avondale, PA) 5880A instrument equipped with a flame-ionization detector, using a temperature gradient from 65 to 150 °C (rate of 7 °C/min).

NMR Spectroscopy. All NMR measurements were performed on a Varian Unity INOVA 500 MHZ spectrometer equipped with three radio frequency channels, 3-axis pulsed-field gradients, and a triple-resonance ^{1}H-detect probe. Protein samples were dissolved in 50 mM sodium phosphate (90% H_2O, 10% D_2O), pH* 6.3, and experiments were recorded at 30 °C, unless otherwise specified. Proton chemical shifts were referenced to external DSS (0 ppm), while ^{15}N and ^{13}C chemical shifts were referenced indirectly to liquid ammonia and tetramethylsilane, respectively (*27, 28*). For ^{15}N-edited experiments, the carrier was placed at 4.73 ppm (^{1}H) and 120 ppm (^{15}N). Triple-resonance experiments were performed with the carrier placed at 4.73 ppm (^{1}H), 118 ppm (^{15}N), 40 ppm ($^{13}C^{\alpha\beta}$), 54 ppm ($^{13}C^{\alpha}$), 35 ppm ($^{13}C^{\beta}$), or 125 ppm (aromatic ^{13}C).

^{1}H−^{15}N HSQC *(29)* spectra were recorded with ^{15}N-labeled 0.5 mM rMUP-I containing various concentrations of the pheromone. A 20 mM solution of 2-*sec*-butyl-4,5-dihydrothiazole was used for titration; 4096 and 512 complex points and spectral widths of 8000 and 2000 Hz were used in the ^{1}H and ^{15}N dimensions, respectively. A refocused HSQC experiment was employed to distinguish between NH_2 vs NH signals (*30*). ^{15}N-edited TOCSY−HSQC (*31*) and NOESY−HSQC (*31*) experiments were recorded with mixing times of 105 and 120 ms, respectively, using ^{15}N-labeled 0.5 mM rMUP-I containing a 2-fold molar excess of the pheromone. Spectral widths of 7000, 6000, and 2000 Hz were employed for direct ^{1}H, indirect ^{1}H, and ^{15}N dimensions, respectively, and 2048 and 32 complex points were recorded in direct ^{1}H and ^{15}N dimensions, respectively. A total of 128 and 96 complex points were recorded in the indirect ^{1}H dimensions of the TOCSY−HSQC and NOESY−HSQC experiments, respectively.

An HNHA experiment was used to measure the ^3J (H^NH^{α}) coupling constants (*32, 33*). The total length of the defocusing and refocusing delays, 2ζ (*33*), was 34.5 ms. The T_{1sel} relaxation time was assumed to be ~100 ms (*33*) as determined for staphylococcal nuclease, a protein of molecular mass comparable to MUP-I (*34*). The HNHA was run with the same sample and parameters as the above ^{15}N-edited 3D experiments, except that 64 complex points were recorded in the indirect ^{1}H dimension. Amide hydrogen exchange rates were monitored by recording a series of 12 min ^{1}H−^{15}N HSQC experiments on a sample freshly exchanged into 50 mM sodium phosphate, pD* 6.3, in 100% D_2O. Buffer exchange was performed on a Pharmacia PD-10 column, followed by concentration in Microcon 10 concentrators.

Triple-resonance CBCA(CO)NH (*35*), HN(CO)CA (*36, 37*), HNCACB (*35*), and HNCA (*38*) spectra were recorded using ^{13}C,^{15}N-labeled 1.1 mM rMUP-I containing a 2-fold molar excess of the pheromone. A total of 512 [HN(CO)CA and CBCA(CO)NH] or 2048 (HNCA and HNCACB) ^{1}H complex points, 50 ^{13}C complex points, and 32 [HNCACB and CBCA(CO)NH] or 44 [HNCA and HN(CO)CA] ^{15}N complex points were acquired. Spectral widths of 8000 (^{1}H), 4000 (^{13}C), and 1800 Hz (^{15}N) were used in the HN(CO)CA and HNCA experiments, while spectral widths of 7000 (^{1}H), 7540 (^{13}C), and 1800 Hz (^{15}N) were used in the CBCA(CO)NH and HNCACB experiments.

HCCH−TOCSY (*39*), (HB)CB(CGCD)HD (*40*), (HB)CB(CGCDCE)HE (*40*), ^{13}C F1-filtered, F3-edited NOESY−HSQC (*41*), and ^{13}C-filtered TOCSY spectra were recorded using ^{13}C,^{15}N-labeled 1 mM rMUP-I containing an equimolar amount of the pheromone. In the (HB)CB(CGCD)HD and (HB)CB(CGCDCE)HE experiments, 256 complex points in the direct (^{1}H) dimension and 24 complex points in the indirect (^{13}C) dimension were recorded using spectral widths of 8000 and 3500 Hz, respectively. In the ^{13}C-filtered TOCSY experiment [a modified version of the ^{13}C F1-filtered, F3-edited NOESY−HSQC (*41*) with the TOCSY pulse sequence replacing the NOESY−HSQC sequence], 2048 complex points in the direct and 256 complex points in the indirect ^{1}H dimension were acquired, using 8000 Hz spectral width in both dimensions. The respective number of complex points in the direct ^{1}H, indirect ^{1}H, and ^{13}C dimensions of the HCCH−TOCSY spectra were 2048, 32, and 32, using spectral widths of 7000 Hz (direct ^{1}H), 7000 Hz (indirect aliphatic ^{1}H) or 3000 Hz (indirect aromatic ^{1}H), and 3000 Hz (^{13}C). The same numbers of complex points were acquired in the ^{13}C F1-filtered, F3-edited NOESY−HSQC experiment using 8000 Hz (direct ^{1}H), 7000 Hz (indirect, ^{13}C-filtered ^{1}H), and 3000 Hz (^{13}C) spectral widths and a mixing time of 150 ms. The ^{13}C carrier was placed at 67 ppm in the ^{13}C-filtered experiments.

Quadrature detection in indirect dimensions was obtained using the States-TPPI method (*42*) with the exception of the indirect ^{1}H dimension of the ^{15}N-edited TOCSY−HSQC for which the States method was used (*43*). A low-pass filter and 3 Hz line broadening in the direct dimension and cosine bell function in the indirect dimensions were applied during data processing on a Silicon Graphics workstation using Felix 95 software (Molecular Simulations, Inc., Burlington, MA).

RESULTS

Protein Expression and Characterization. The MUP-I expression construct was designed to produce a polypeptide with the MUP-I signal sequence replaced by a hexahistidine tag. A factor Xa cleavage site preceding the first MUP-I residue provided means of producing a protein with a native N-terminus. The expression and purification protocol yielded approximately 15 mg of the purified rMUP-I from a 1 L culture. The protein exhibited identical isoelectric point, SDS−PAGE migration, and anion-exchange chromatography elution time to the major component of the authentic MUP from male mouse urine (data not shown). The mass of 18 692 Daltons, determined through MALDI-TOF-MS, is identical to the expected mass of 18 694 Daltons (*12*) within the experimental error of 0.02%. The ligand binding affinity of the recombinant protein was slightly higher than measured with a protein isolated from the urine, as will be discussed below. Thus, a protein identical with the mammalian MUP-I form can be produced in bacteria.

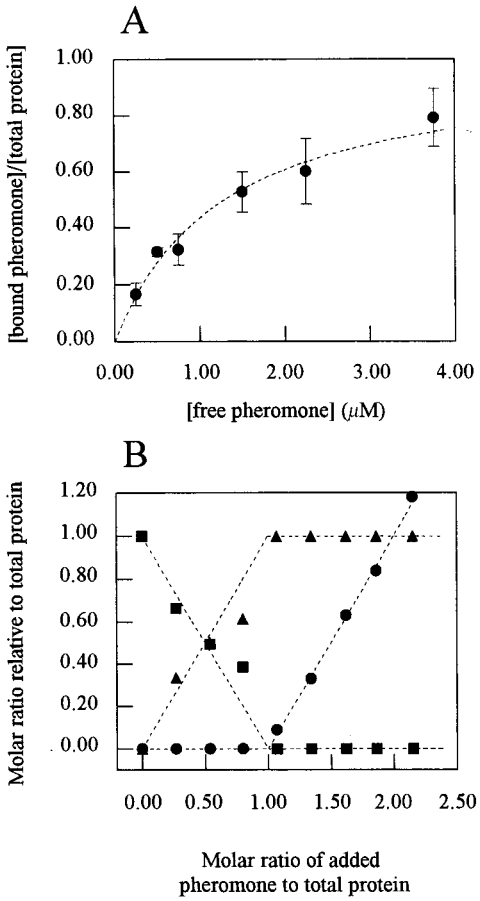

FIGURE 1: (A) Binding curve for racemic 2-*sec*-butyl-4,5-dihydrothiazole binding to rMUP-I. Data points are the averages, and error bars are the standard deviations of 3 or 4 independent measurements. (B) NMR titration at 30 °C of rMUP-I with 2-*sec*-butyl-4,5-dihydrothiazole (circles, free pheromone; squares, free protein; and triangles, protein−pheromone complex). Areas of the methyl 9 proton peak of the free pheromone in 1D ^{1}H spectra and volumes of Tyr 84 amide peaks in ^{1}H−^{15}N HSQC spectra were used as measures of concentration and normalized to the total protein concentration. Dashed lines indicate the theoretical curves expected for 1:1 stoichiometry of racemic pheromone to protein.

Dissociation Constant, Stoichiometry, and Exchange Rate of the Pheromone/MUP-I Complex. The dissociation constant of the 2-*sec*-butyl-4,5-dihydrothiazole/rMUP-I complex was determined by a diffusion method with gas chromatographic detection. Nonlinear curve fitting of the binding data (Figure 1A) gave a dissociation constant of 1.3 ± 0.1 μM. Binding stoichiometry, determined at a high pheromone concentration (data not shown), was 1.0 ± 0.1 racemic pheromone molecule per protein molecule. The results of the binding studies indicate that the overexpressed protein is properly folded and exhibits characteristics of the native pheromone binding urinary protein.

The stoichiometry of 2-*sec*-butyl-4,5-dihydrothiazole binding to rMUP-I was also determined by 2D NMR spectroscopy. As the pheromone concentration increased, new peaks appeared in the ^{1}H−^{15}N HSQC spectrum. In several cases, well-separated pairs of original, free protein signals and new signals of protein−pheromone complex allowed the bound-to-free protein ratio to be monitored (Figure 2). Intensities of free protein peaks disappeared and bound protein peaks reached maximum intensity at a racemic pheromone:protein ratio of 1:1, in good agreement with the stoichiometry measured gas chromatographically (Figure 1B). At higher pheromone concentration, sharp peaks of free 2-*sec*-butyl-4,5-dihydrothiazole became visible in 1D ^{1}H spectra with an area proportional to the excess of the pheromone (Figure 1B). The increase in the free pheromone signal was linear up to a 6-fold excess (data not shown). Similar results were obtained at 15, 30, and 45 °C.

The well-resolved pairs of signals in the ^{1}H−^{15}N HSQC spectrum of rMUP with 0.5 equiv of the pheromone (see example in Figure 2B) indicate that the free protein is in slow exchange with the pheromone−protein complex. The fact that the individual peaks are well-resolved for pairs separated by 50 Hz showed that the off-rate constant was much lower than 50 s^{-1}. This conclusion is supported by the free pheromone signal in 1D proton spectra, where no line broadening or chemical shift change was observed down to approximately 20% molar excess of the pheromone; the line width of the observed signal was 2 Hz.

Interestingly, some amide signals of the saturated pheromone−protein complex (Figure 2C) are not present as single peaks, but instead appear as two peaks of identical intensity separated by 5−35 Hz (i.e., 0.01−0.07 ppm in the ^{1}H dimension or 0.1−0.7 ppm in the ^{15}N dimension). These pairs of peaks were seen only in the spectra of the protein complexed with the racemic pheromone, but not in the spectra obtained using an achiral isobutyl analogue (Figure 2D), which binds to rMUP-I with a dissociation constant of 0.6 ± 0.2 μM (unpublished results). Interpretation of this phenomenon is discussed below.

Identification of the Pheromone Binding Site. ^{1}H−^{15}N HSQC spectra with well-separated signals of the free protein and the pheromone−protein complex offered an opportunity to identify the protein residues in the pheromone binding site. Assignment of the ^{1}H−^{15}N HSQC peaks was accomplished using a sample of ^{13}C,^{15}N-doubly-labeled rMUP-I in complex with a 2-fold molar excess of 2-*sec*-butyl-4,5-dihydrothiazole. The backbone assignments were based mainly on the triple-resonance experiments listed under Materials and Methods. Representative regions of the HNCACB and CBCA(CO)NH spectra, demonstrating the sequential connectivities, are shown in Figure 3. Despite the low intensities of some signals (mostly those affected by the pheromone binding), all ^{1}H−^{15}N HSQC peaks could be assigned (Figure 4). Two complete and several partial overlaps in the ^{1}H−^{15}N HSQC spectrum were clearly separated in the carbon dimension (data not shown). ^{15}N TOCSY−HSQC and NOESY−HSQC spectra provided supporting information for the backbone assignments in ambiguous cases. More than 90% of $d_{\alpha N}(i,i+1)$ NOE transfers were observed and used to confirm the backbone connectivities. ^{1}H−^{15}N HSQC signals of the free protein were assigned by comparison with the HSQC spectrum of the complex and confirmed using a ^{15}N TOCSY−HSQC experiment.

For reliable interpretation of the current results, it is important to establish that the structure of MUP-I does not change significantly between the crystal and solution states. Figure 5 summarizes hydrogen exchange rates, ^3J (H^NH^α) coupling constants, sequential and medium-range NOEs, and secondary chemical shifts (*44*, *45*) in the MUP-I−pheromone complex and compares the secondary structure of MUP-I derived from these solution parameters with the secondary

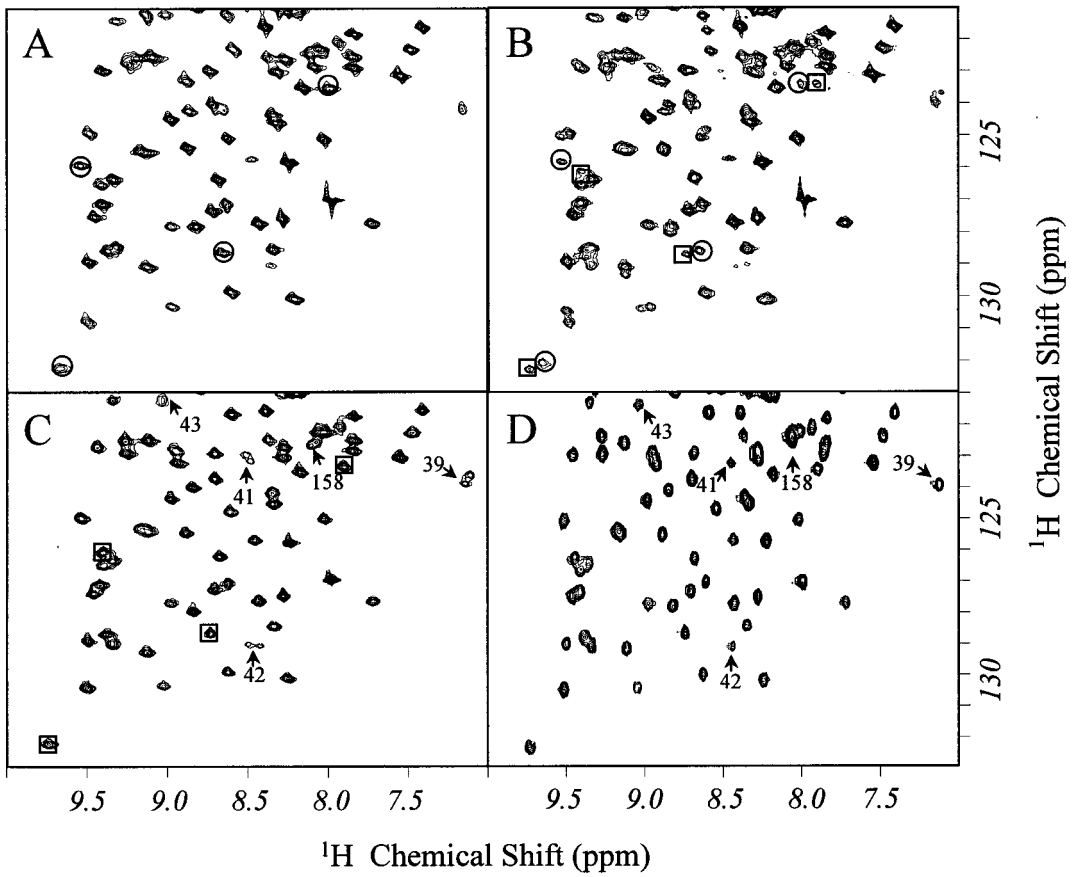

FIGURE 2: Details of ^{1}H−^{15}N HSQC spectra of rMUP-I with (A) 0, (B) 0.5, and (C) 2.0 molar equiv of 2-*sec*-butyl-4,5-dihydrothiazole. Panel D shows a spectrum corresponding to (C) but obtained with the nonchiral analogue 2-isobutyl-4,5-dihydrothiazole as the ligand. Examples of well-resolved peaks corresponding to free protein (circles) and to protein−pheromone complex (boxes) are marked in panels A−C. Peaks split into pairs in the saturated protein−pheromone complex are indicated with arrows and labeled with the corresponding residue numbers. Labeled arrows in panel D indicate that the corresponding peaks are not split when the ligand is nonchiral.

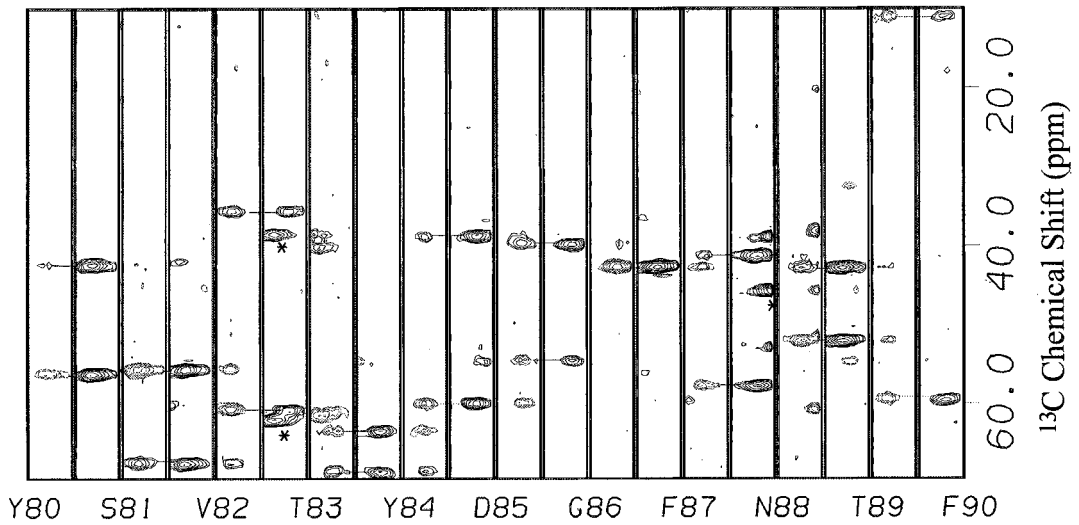

FIGURE 3: Strips taken from the CBCA(CO)NH (left from the residue label) and HNCACB (right from the residue label) spectra at the amide ^{1}H and ^{15}N chemical shifts of residues 80−90. Horizontal lines indicate sequential connectivities, and asterisks mark the overlapping peaks (in ^{1}H and ^{15}N dimensions). Positive peaks are shown as solid contours, and negative peaks are shown as dotted contours.

structure of MUP determined in the crystal (*14*). The solution data support the existence of the eight β-strands, a long α-helix (residues 128−139), and a short 3_{10}-helix (residues 12−15) that exist in the crystal structure. Interstrand d_{NN} NOEs confirmed folding of the β-sheets into the lipocalin barrel. In particular, NOEs between strands A and H indicated that the barrel was closed. Several expected interstrand $d_{\alpha N}$ NOE transfers were also observed, but their assignment was often equivocal due to resonance overlap (data not shown). An additional turn of helix present in the crystal structure (residues 29−32) may also be present in solution but cannot be unequivocally identified based on the current data. The expected tertiary structure was further supported by the existence of a disulfide bond between Cys-

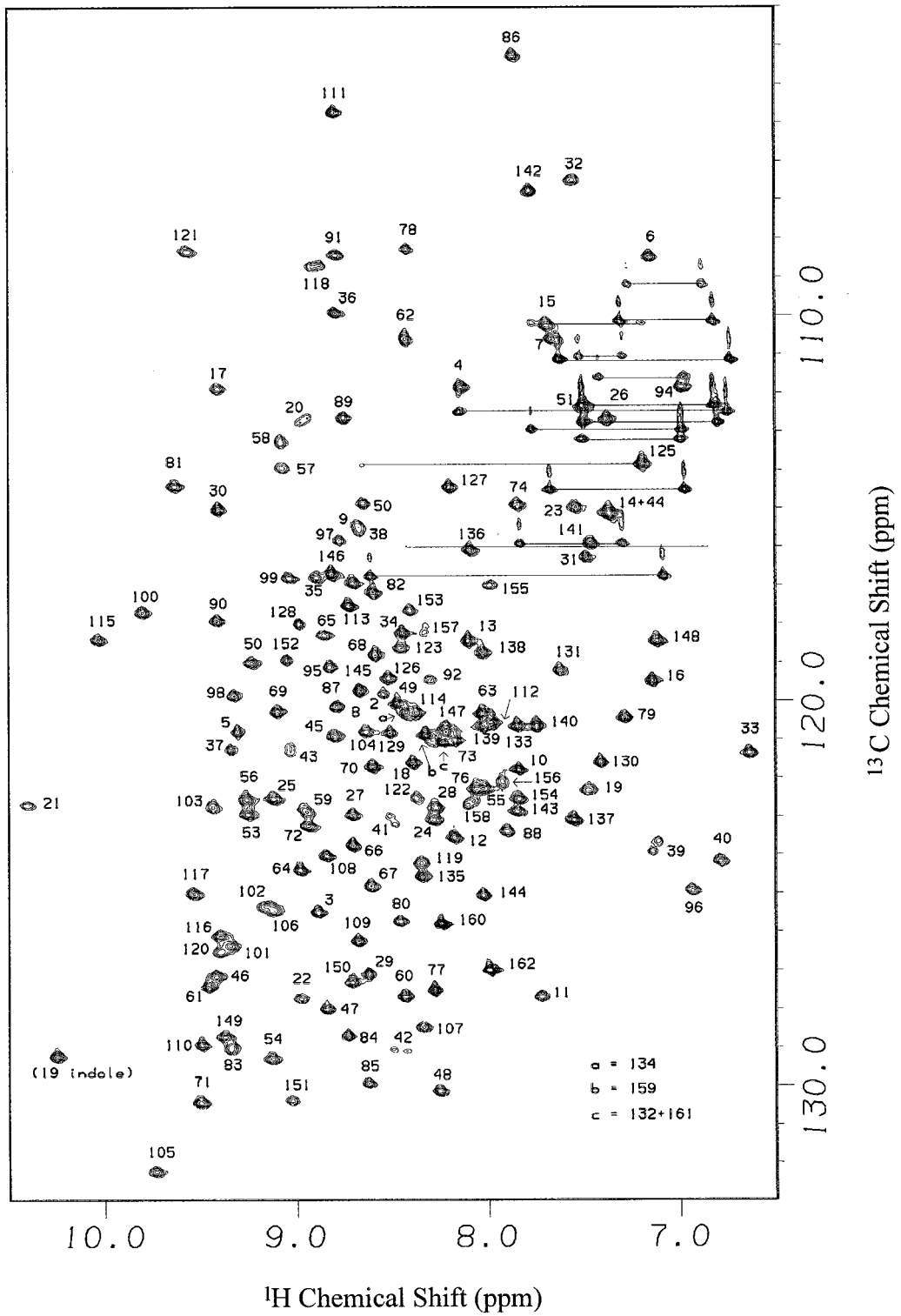

FIGURE 4: ^{1}H−^{15}N HSQC spectrum of pheromone-bound rMUP-I indicating the residue number of each backbone amide resonance. The pairs of correlations connected with horizontal lines correspond to glutamine and asparagine side-chain amide resonances.

64 and Cys-157, as indicated by the C_β chemical shifts of these residues (45.3 and 41.3 ppm, respectively); the C_β chemical shift of Cys-138 is 25.6 ppm, indicating that this cysteine is not disulfide-bonded. Thus, the NMR data confirmed that the secondary and tertiary structures of MUP-I are very similar or identical in the solution and crystalline states. It was therefore reasonable to interpret the ligand interactions observed in solution by comparison with the X-ray structure.

^{1}H−^{15}N HSQC spectra of the free protein and of the pheromone−protein complex were compared in order to identify backbone amide groups affected by pheromone binding. These groups are expected either to be adjacent to the pheromone binding site or to be in areas of the protein whose structures are perturbed as a result of ligand binding (*46*). The peaks most significantly shifted after addition of pheromone are listed in Table 1. A list of the backbone NH groups which appeared as pairs of peaks in the ^{1}H−^{15}N

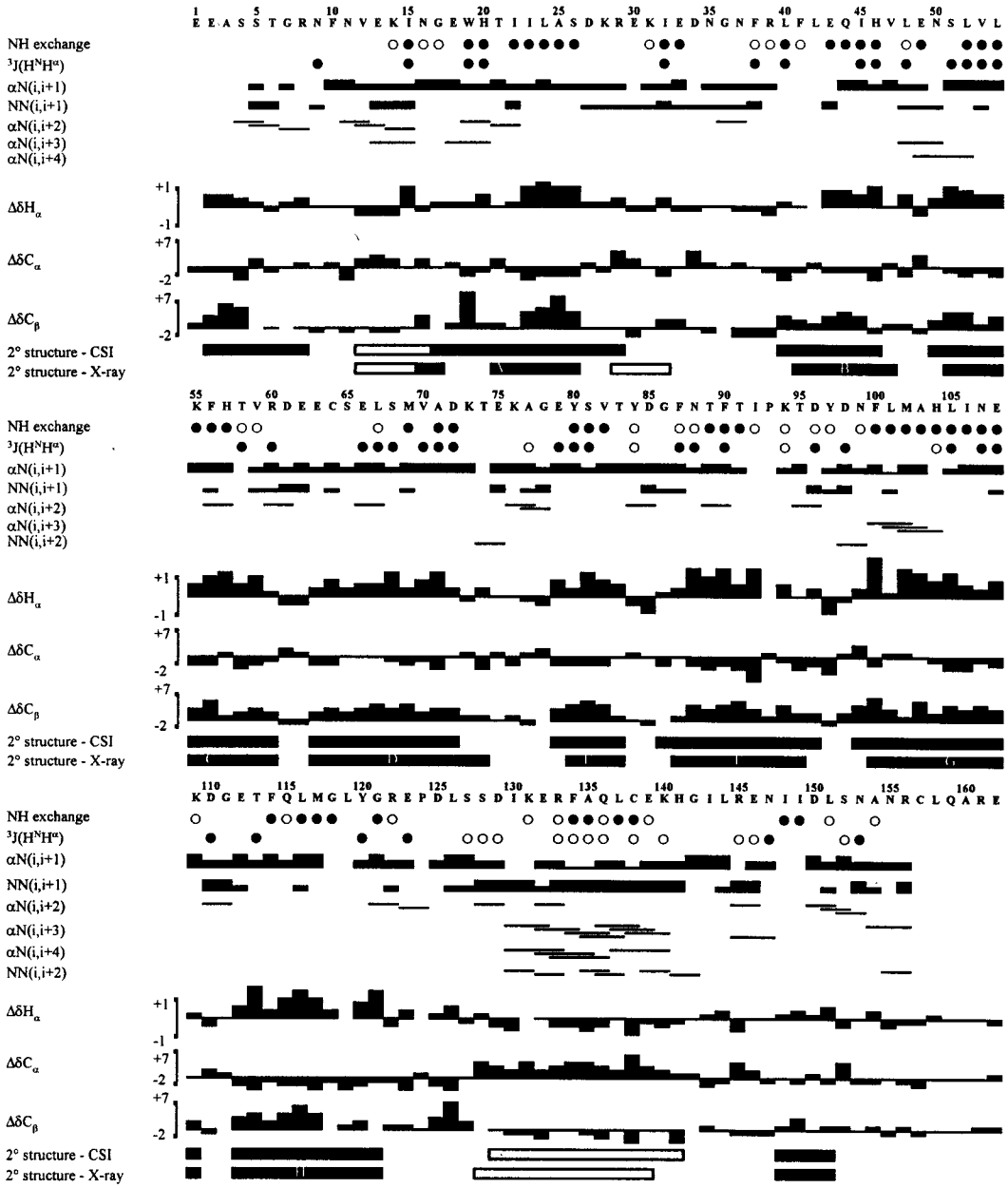

FIGURE 5: Amino acid sequence and summary of NMR data used for secondary structure confirmation. Slowly exchanging amide protons (retained after 18 h) are indicated by filled circles, and amide protons with an intermediate exchange rate (retained after 1 h) are indicated with open circles. ^3J (H^NH^α) values greater than 8 Hz and smaller than 5 Hz are indicated by filled and open circles, respectively. The strength of sequential NOEs is represented by line thickness. The secondary chemical shift histograms show deviations in ppm from average "random coil" values (*44*, *45*). Secondary structure elements predicted from the consensus chemical shift indices and those identified from crystallographic data *(14)* are shown at the bottom (upper and lower lines, respectively); helices are indicated in white and strands in black.

HSQC spectrum of the pheromone−protein complex is presented in Table 2. Intensities of the individual signals in these pairs were always of the same magnitude (less than 10% difference).

To identify interactions of the bound pheromone with individual residues of the binding site, ligand-to-protein NOEs were measured in a ^{13}C F1-filtered, F3-edited NOESY−HSQC experiment (*41*). Resonances of the pheromone protons, attached to ^{12}C, were assigned using a ^{13}C-filtered TOCSY experiment (Figure 6B). The assignment of the bound pheromone peaks was based on the observed TOCSY connectivities and on comparison of chemical shifts to the spectrum of the free compound (Figure 6A). As indicated in Figure 6B, peaks attributed to the *sec*-butyl group formed two overlapping spin systems corresponding to two forms of the bound ligand (labeled a and b). The assignment of CH_2-4 and CH_2-5 was based on their chemical shifts (downfield chemical shift assigned to CH_2-4 as in the free pheromone).

Resonances corresponding to protein side chain groups in the binding cavity were assigned using HCCH−TOCSY (*39*) experiments in combination with the 2D experiments correlating aromatic protons to $^{13}C^\beta$ (see Materials and Methods).

The interpretation of the ^{13}C F1-filtered, F3-edited NOESY−HSQC spectra focused on methyl groups and aromatic protons of the protein. The aliphatic region of the spectrum was partially obscured by a diagonal background of incompletely filtered intramolecular protein NOEs. Nevertheless, multiple intermolecular NOEs were identified in the upfield

Table 1: MUP-I Backbone Amide Resonances Shifted upon Pheromone Binding

	chemical shift difference (ppm)[a]	
residue	^{1}H	^{15}N
Phe 41[b]	0.12	1.2
	0.16	1.0
Val 59	0.12	0.3
Met 69	0.03	1.0
Val 70	0.01	1.0
Asn 88	0.14	0.1
Thr 89	0.00	1.1
Phe 90	0.01	2.2
Thr 91	0.10	2.2
His 104	0.03	1.0
Leu 116	0.17	0.2

[a] Listed for each NH group is the chemical shift change (absolute value) observed upon pheromone binding. [b] Two NH resonances were observed for Phe 41 in the pheromone − MUP-I complex (see Table 2).

Table 2: MUP-I Backbone Amide Groups Appearing as Pairs of Peaks in the $^{1}H-^{15}N$ Spectrum

	chemical shift separation (ppm)[a]	
residue	^{1}H	^{15}N
His 20	0.04	0.1
Arg 39	0.03	0.3
Phe 41	0.03	0.2
Leu 42	0.07	0.0
Glu 43	0.00	0.1
Gly 118	0.03	0.0
Cys 157	0.02	0.1
Leu 158	0.04	0.2

[a] Values listed are separations between pairs of equally intense peaks observed for each residue in the spectrum of the pheromone−MUP-I complex.

portion of the spectrum. The NOEs observed in the aromatic region were weaker, but significantly less affected by the background. Protein protons with NOEs to the pheromone were identified in the 3D spectrum by their chemical shifts and the chemical shifts of the attached carbon atoms. All NOEs were verified by comparison to a control spectrum recorded in the absence of the ligand. However, possible changes of the background due to ligand binding require some peaks close to the regions of high background to be interpreted with caution, as indicated in Table 3. Four representative strips of the ^{13}C F1-filtered, F3-edited NOESY−HSQC spectrum and corresponding strips from the control spectrum are shown in Figure 7.

A list of observed intermolecular NOEs is presented in Table 3. The observed NOEs were separated into two groups, reflecting proximity either to the dihydrothiazole ring or to the *sec*-butyl chain. The NOEs showed that residues 42, 54, 90, 103, and 120 were close to the *sec*-butyl group, residues 40, 69, 82, 84, and 105 were close to the dihydrothiazole ring, and residue 56 exhibited NOEs to both parts of the ligand molecule. These data allowed the approximate orientation of the pheromone in the binding pocket to be readily determined.

DISCUSSION

The previously reported X-ray structure of a MUP crystallized from a fractionated mouse urine sample (*14*) provided

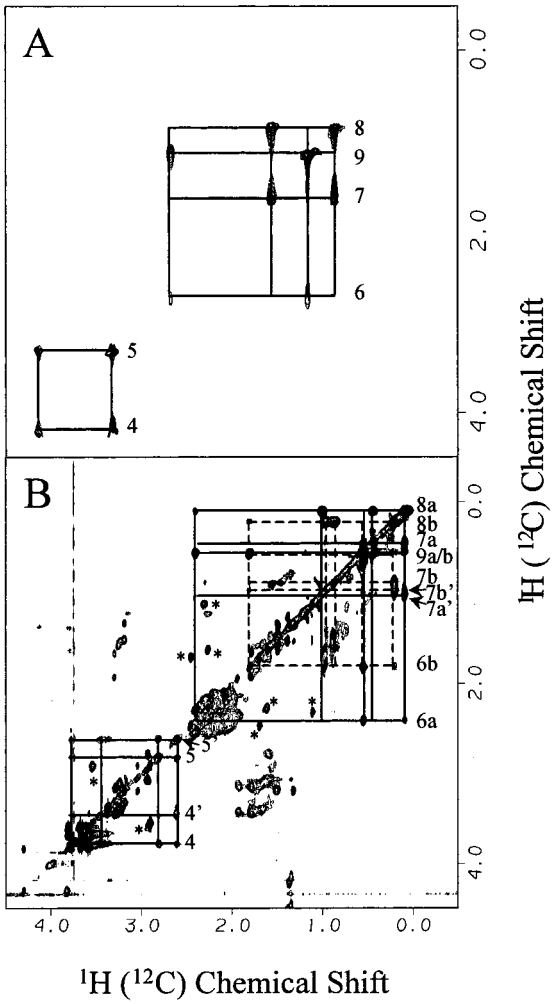

FIGURE 6: ^{13}C-filtered TOCSY spectra of (A) 5.7 mM free 2-*sec*-butyl-4,5-dihydrothiazole and (B) 1 mM 2-*sec*-butyl-4,5-dihydrothiazole/rMUP-I complex (B). In panel B, cross-peaks of the *sec*-butyl groups of the two different ligand forms are distinguished by connecting lines (a, solid; and b, dashed). Cross-peaks marked with asterisks are attributed to minor impurities that do not bind to MUP-I and therefore give sharp peaks relative to the protein-bound pheromone. The symbols a and b in the proton labels refer to individual *sec*-butyl spin systems, and diastereotopic protons are distinguished with a prime.

the first structural details about the urinary pheromone binding proteins. The electron density localized in the proposed binding pocket indicated the presence of a natural ligand, but its shape could not be identified unequivocally. Although Böcskei et al. (*14*) interpreted the bound molecule as 2-*sec*-butyl-4,5-dihydrothiazole with the structure fitting the binding site reasonably well, the ligand was not included in either the refinement or the map calculation. The precise orientation of the ligand and its attribution to 2-*sec*-butyl-4,5-dihydrothiazole thus remained ambiguous given the resolution of that structure and the ability of other low-molecular-weight urinary components to bind to MUP (*20*). The ambiguity was further magnified by the heterogeneity of the MUP fraction. There are several MUPs that could possibly contaminate the MUP crystal (*12*). In the present study, the natural material was replaced by a well-defined complex of the recombinant protein with synthetic pheromone. The protein, rMUP-I, was prepared in a bacterial expression system, and its identity with the native protein was verified by several methods. The established dissociation

Table 3: Intermolecular NOEs between 2-*sec*-Butyl-4,5-dihydrothiazole and MUP-I[a]

	ligand									
	sec-butyl chain protons[b]						dihydrothiazole ring protons[b]			
protein	9a/b	8a	8b	7a	7b	7a′/7b′	5	5′	4	4′
Leu 42δ_1	w[c]	x	x	m	x	m[d]				
Leu 42δ_2	m	s				m				
Ala 103β	vs[d]	s[d]	w[c]	w[c]	x	x				
Leu 54δ_1	x	w[c]	s[d]	x	m[c]	m				
Leu 54δ_2	x	w[c]	s[d]	x	x	x				
Tyr 120ϵ_2	m	m								
Phe 90δ_2	m			w[c]						
Phe 90ϵ_2						m				
Phe 56ϵ_2	w				m[d]	m				
Phe 56ζ	m			w[c]		m	m[d]		m[d]	
Leu 105δ_1	x			x	x	x	w	m	m	w
Leu 40δ_1	x			x			m	m	s	s
Val 82γ_1	x	x	x	x	x	x	m	m		
Met 69ϵ	x	x	x	x	x	x	s	w	w	m
Tyr 84δ_2							m	w[c]		

[a] Strength of the NOEs is expressed in a semiquantitative manner (vs, very strong; s, strong; m, medium; w, weak; and x, obscured by background). [b] The symbols a and b in the proton labels refer to individual *sec*-butyl spin systems and diastereotopic protons are distinguished with a prime as indicated in Figure 6B. [c] Possible weak signal obscured by a close intense NOE peak. [d] Medium or intense peaks close to an area of high background.

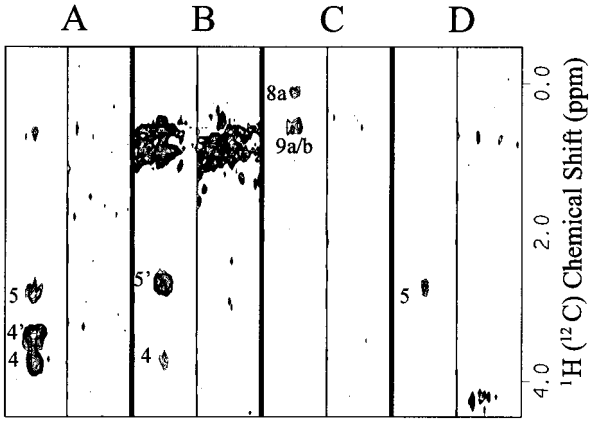

FIGURE 7: Representative strips from ^{13}C F1-filtered, F3-edited NOESY−HSQC spectra of free (right strips) and 2-*sec*-butyl-4,5-dihydrothiazole-complexed (left strips) rMUP-I. The strips were taken from the 3D spectra at chemical shift values corresponding to (A) Leu 40δ_1, (B) Leu 105δ_1, (C) Tyr 120ϵ_2, and (D) Tyr 84δ_2. The NOE cross-peaks are labeled with the corresponding ligand proton numbers.

constant determined here was 8 times lower than the 10 ± 3 μM value published by Bacchini et al. (*21*) for the MUP complex isolated from urine. The slightly higher apparent dissociation constant of the urinary complex may reflect the presence of MUP species of lower binding affinity in the natural sample. It is noteworthy that the concentrations of MUP and pheromone in urine are ~100 μM and ~10 μM, respectively (*21*), suggesting that most of the pheromone in the urine is bound to MUP. The recombinant protein provided an opportunity to study 2-*sec*-butyl-4,5-dihydrothiazole binding under well-defined conditions.

The effects of the pheromone binding on the well-resolved amide signals were observed in ^{1}H−^{15}N correlation spectra. Titration of the protein with the ligand, monitored by NMR spectroscopy, showed that the pheromone−ligand complex and the free protein are in slow exchange on the NMR chemical shift time scale. The relatively low off-rate constant is typical for protein−ligand complexes with micromolar dissociation constants (*47*). Slow dissociation may be important for the proposed pheromone-releasing function of MUPs (*15*).

The shape of the titration curves in Figure 1 is somewhat unexpected. Although a racemic mixture of 2-*sec*-butyl-4,5-dihydrothiazole was used, the titration curve does not exhibit any discrimination between the enantiomers. The absence of the free pheromone signal up to 1:1 ligand:protein ratio is consistent with a 1:1 binding stoichiometry of racemic pheromone to protein, as observed in the diffusion binding assay. If a single enantiomer were bound, the free pheromone signal would be expected to increase with a slope of 0.5 until reaching a 2:1 ligand:protein ratio; then, the signal would continue to increase with a slope of unity. Deuterium exchange data (*24*) showed that 2-*sec*-butyl-4,5-dihydrothiazole can racemize easily and that pure enantiomers are practically inaccessible. However, this racemization is too slow (exchange rate much lower than 1 h^{-1}) to explain the absence of a nonbinding species. The ability of rMUP-I to bind either enatiomer seems to be a more probable interpretation. MUPs and related proteins exhibit a relatively low ligand specificity (*15*, *21*). It should be noted that 2-*sec*-butyl-4,5-dihydrothiazole has been isolated from the natural protein as a racemic mixture (*24*) which makes the use of a racemic pheromone biologically relevant.

Further analysis of the NMR spectra confirmed the presence of two equally populated states of the protein−pheromone complex. Several ^{1}H−^{15}N HSQC peaks were split into pairs separated by 0.01−0.07 ppm in the ^{1}H dimension or 0.1−0.7 ppm in the ^{15}N dimension after the pheromone binding (Figure 2C and Table 2). Significantly, all of the NH groups whose signals are split in this way are located on one side of the hydrophobic binding cavity (Figure 8). They include Arg 39, Phe 41, Leu 42, and Glu 43 at the beginning of strand B and His 20 and Gly 118 in adjacent strands A and H, respectively (see Figure 5 for strand labeling).

The presence of two equally populated forms of the bound ligand was also evident from the ^{13}C-filtered TOCSY spectrum (Figure 6) showing two spin systems for the *sec*-butyl side chain. The largest differences in chemical shift were observed for protons attached to C-6 (the chiral carbon atom) and C-7. On the other hand, a single cross-peak set was identified for protons attached to the dihydrothiazole ring. Taken together, the titration results and the splitting of both protein and ligand resonances into equally populated pairs are most readily interpreted by proposing that both enantiomers of the pheromone bind to MUP-I with approximately equal affinity and slow exchange binding kinetics. More complex possibilities, invoking separate binding and conformational rearrangement steps, can be put forward, but the proposal that the peak splitting results from the binding of both enantiomers is the simplest explanation of the current data. If this hypothesis is correct, one would expect a nonchiral pheromone analogue to cause similar changes in protein chemical shifts upon binding (compared with 2-*sec*-butyl-4,5-dihydrothiazole) but not to result in splitting of resonances in the saturated complex. Indeed, the achiral analogue 2-isobutyl-4,5-dihydrothiazole, which binds

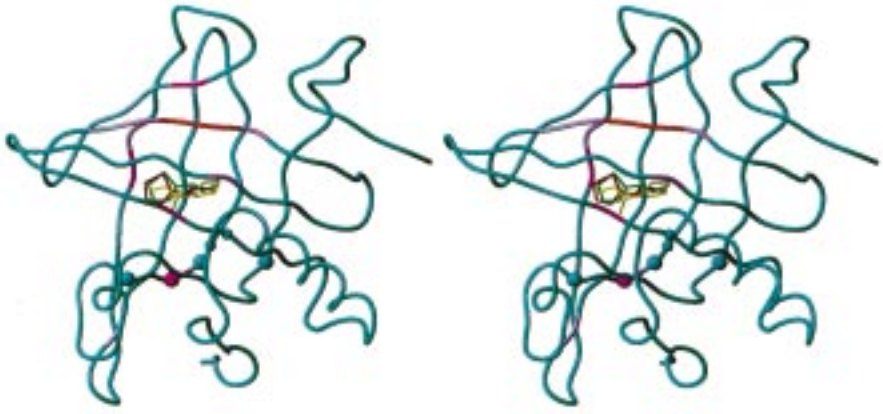

FIGURE 8: Models of the complexes between the pheromone and rMUP-I, shown in stereo. The coordinates of the protein are taken from the crystal structure (PDB code 1mup, ref *14*). The positions of the ligand *S* and *R* enantiomers modeled here are shown in red and green, respectively, whereas the position of the *S* enantiomer modeled by Böcskei et al. *(14)* is shown in yellow. The protein backbone is represented on a continuous red−blue color scale indicating the change in backbone amide chemical shift of each residue in response to pheromone binding; red indicates maximum change, and blue indicates no change. Amide groups whose resonances are split into pairs in the HSQC spectrum are shown as spheres with the magnitude of the splitting indicated by the sphere radius. The models shown here were obtained as follows. Each enantiomer was manually docked to the protein in an orientation that satisfied most of the intermolecular NOEs. An exhaustive conformational search was performed using molecular dynamics (1000 K; 10 ps equilibration; 200 structures collected and energy-minimized at 2 ps intervals; restrained by the unequivocal NOEs in Table 3). The two structures shown are representatives of the ensemble that satisfies the NOEs listed in Table 3, based on the assignment that spin systems a and b represent the *S* and *R* enantiomers, respectively.

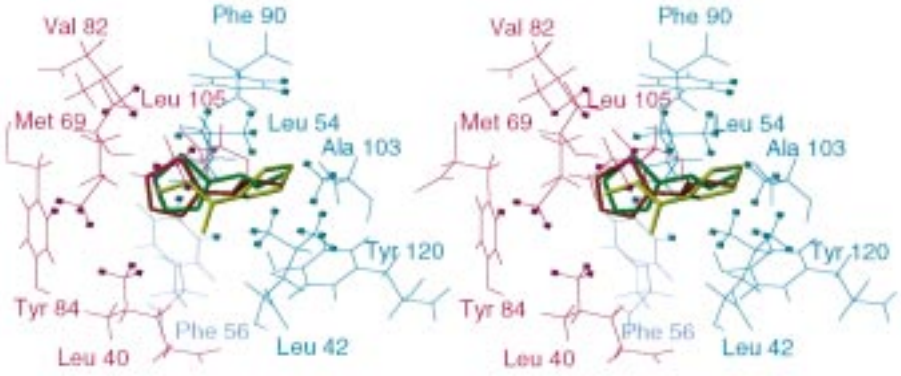

FIGURE 9: Detailed stereo representation of the binding site in the protein−pheromone complexes shown in Figure 8. Ligand color coding is the same as in Figure 8. Protein residues that exhibit intermolecular NOEs to the pheromone are colored in magenta (NOEs to the dihydrothiazole), cyan (NOEs to the *sec*-butyl group), or purple (NOEs to both); specific protons involved in these NOEs are highlighted.

to MUP-I with comparable affinity to 2-*sec*-butyl-4,5-dihydrothiazole, shows exactly this type of behavior (Figure 2D).

The fact that the pheromone binding significantly affected only a limited number of amide peaks allowed the binding site to be mapped (*46*). The largest chemical shift changes occurred for NH groups in β-strands D, E, F, and G which are located on one side of the hydrophobic cavity (Figure 8). In addition, significant shifts were observed for NH groups near the N-terminus of β-strand B and the C-terminus of β-strand C, which are located on the opposite side of the barrel from the other shifted groups. This confirms that the bound pheromone is located near the middle of the barrel (Figure 8; see Figure 5 for strand labeling). Peripheral regions of the protein, e.g., the long helix, remained almost unaffected.

The position of the ligand within the binding cavity of MUP-I was further investigated in the ^{13}C-filtered NOESY experiment. Analysis of the NOE data revealed that the orientation of the ligand occupying the binding cavity differed from that proposed by Böcskei et al. (*14*). In the previous model, the dihydrothiazole ring occupies a pocket lined by the side chains of Leu 42, Leu 54, Phe 90, Ala 103, and Tyr 120 while the *sec*-butyl chain was oriented toward Leu 40, Tyr 84, and Met 69. In contrast, our NOE data indicate that the dihydrothiazole ring is adjacent to residue 40 whereas the *sec*-butyl chain approaches the side chains of residues 42, 54, 90, 103, and 120 in one or both diastereomeric complexes. Thus, the current data are inconsistent with the reported ligand orientation but instead indicate that the positions of the ring and the *sec*-butyl chain are reversed relative to the crystal structure (Figure 9). A recent high-resolution X-ray analysis of the complex between rMUP-I and 2-*sec*-butyl-4,5-dihydrothiazole is consistent with the orientation found in the current NMR study (D. Timm, personal communication).

Although the relative orientations of the dihydrothiazole ring and the *sec*-butyl group are clearly defined by the NOE data, the precise positions of the methyl and ethyl substituents of the chiral carbon (C-6) are more difficult to identify due to the presence of both ligand enantiomers in the NMR samples of the complex. Assuming that each enantiomer was

rigidly fixed in its optimal conformation, it was possible to identify a ligand orientation that satisfied all of the observed NOEs if forms a and b were assigned to enantiomers *S* and *R*, respectively, but not if the alternative stereospecific assignment was made. However, the alternative assignment remains possible if free rotation about the C6−C8 and/or C2−C6 bonds occur in the protein-bound pheromone.

Models of the protein−pheromone complexes compatible with the observed NMR data are presented for each enentiomer in Figure 8. In each complex, the pheromone is located in the middle of the eight-stranded β-barrel. Most of the residues whose NH groups exhibit significant chemical shift changes upon pheromone binding are located in the β-strands on the top side of the barrel as depicted in Figure 8. These residues cover the whole length of the bound pheromone in the models. The NH groups whose resonances become split upon pheromone binding form a curved surface at the bottom right-hand region of the binding cavity as depicted in Figure 8. These include the NH groups of residues 41, 42, and 43, which most closely approach the chiral center of the ligand. A detailed view of these models, highlighting the amino acid side chains that exhibit the NOEs to the bound pheromone, is shown in Figure 9. Amino acids showing NOEs to the dihydrothiazole ring are clustered on the left-hand side of this view whereas those showing NOEs to the *sec*-butyl portion of the ligand are clustered on the right. This view provides convincing evidence that the orientation of the pheromone in the binding pocket is opposite to the orientation modeled previously (*14*).

In summary, we have used NMR spectroscopy to monitor the interaction between recombinant MUP-1 and the synthetic pheromonal ligand 2-*sec*-butyl-4,5-dihydrothiazole. The secondary structure of the protein in solution is very similar to that in the crystal state (*14*). The protein binds racemic pheromone with a stoichiometry of 1:1. Protein chemical shift changes upon pheromone binding and intermolecular NOEs allowed the ligand binding cavity to be identified. The orientation of the pheromone in the protein binding site, revealed using isotope-filtered NOESY experiments, differs significantly from that proposed previously (*14*).

ACKNOWLEDGMENT

We are grateful to Dr. John Bishop for providing the cLiv1 gene, to Dr. Lewis E. Kay for pulse-sequence programs, and to the Indiana University NMR facility for technical support. We also thank Drs. Kristen L. Mayer and Jiqing Ye for assistance in implementation of NMR pulse sequences and Dr. David Timm for helpful discussions.

REFERENCES

1. Finlayson, J. S., Potter, M., and Runner, R. C. (1963) *J. Natl. Cancer Inst. 31*, 91−107.
2. Bishop, J. O., Clark, A. J., Clissold, P. M., Hainey, S., and Francke, U. (1982) *EMBO J. 1*, 615−620.
3. Clissold, P. M., and Bishop, J. O. (1982) *Gene 18*, 211−220.
4. Held, W. A., Gallagher, J. F., Hohman, C. M., Kuhn, N. J., Sampsel, B. M., and Hughes, R. G., Jr. (1987) *Mol. Cell. Biol. 7*, 3705−3712.
5. Al-Shawi, R., Ghazal, P., Clark, A. J., and Bishop, J. O. (1989) *J. Mol. Evol. 29*, 302−313.
6. Kuhn, N. J., Woodworth-Gutai, M., Gross, K. W., and Held, W. A. (1984) *Nucleic Acids Res. 12*, 6073−6090.
7. Knopf, J. L., Gallagher, J. F., and Held, W. A. (1983) *Mol. Cell. Biol. 3*, 2232−2240.
8. Shahan, K. M., Gilmartin, M., and Derman, E. (1987) *Mol. Cell. Biol. 7*, 1938−1946.
9. Shahan, K., Denaro, M., Gilmartin, M., Shi, Y., and Derman, E. (1987) *Mol. Cell. Biol. 7*, 1947−1954.
10. Shaw, P. H., Held, W. A., and Hastie, N. D. (1983) *Cell 32*, 755−761.
11. Evershed, R. P., Robertson, D. H. L., Beynon, R. J., and Green, B. N. (1993) *Rapid Commun. Mass Spectrom. 7*, 882−886.
12. Robertson, D. H. L., Cox, K. A., Gaskell, S. J., Evershed, R. P., and Beynon, R. J. (1996) *Biochem. J. 316*, 265−272.
13. Robertson, D. H. L., Hurst, J. L., Bolgar, M. S., Gaskell, S. J., and Beynon, R. J. (1997) *Rapid Commun. Mass Spectrom. 11*, 786−790.
14. Böcskei, Z., Groom, C. R., Flower, D. R., Wrigth, C. E., Phillips, S. E. V., Cavaggioni, A., Findlay, J. B. C., and North, A. C. T. (1992) *Nature 360*, 186−188.
15. Beynon, R. J., Robertson, D. H. L., Hubbard, S. J., Gaskell, S. J., and Hurst, J. L. (1997) in *Abstracts of the 8th Chemical Signals in Vertebrates Symposium*, p 4, Cornell University, Ithaca, NY.
16. Novotny, M. V., Jemiolo, B., and Harvey, S. (1990) in *Chemical Signals in Vertebrates 5* (MacDonald, D. W., Müller-Schwartze, D., and Natynczuk, S., Eds.) pp 1−22, Oxford University Press, Oxford, U.K.
17. Novotny, M. V., Harvey, S., Jemiolo, B., and Alberts, J. (1985) *Proc. Natl. Acad. Sci. U.S.A. 82*, 2059−2061.
18. Jemiolo, B., Harvey, S., and Novotny, M. V. (1986) *Proc. Natl. Acad. Sci. U.S.A. 83*, 4576−4579.
19. Novotny, M. V., Jemiolo, B., Harvey, S., Wiesler, D., and Marchlewska-Koj, A. (1986) *Science 231*, 722.
20. Robertson, D. H. L., Beynon, R. J., and Evershed, R. P. (1993) *J. Chem. Ecol. 19*, 1405−1416.
21. Bacchini, A., Gaetani, E., and Cavaggioni, A. (1992) *Experientia 48*, 419−421.
22. Flower, D. R. (1996) *Biochem. J. 318*, 1−14.
23. Ferrari, E., Lodi, T., Sorbi, R. T., Tirindelli, R., Cavaggioni, A., and Spisni, A. (1997) *FEBS Lett. 401*, 73−77.
24. Novotny, M. V., Xie, T.-M., Harvey, S., Wiesler, D., Jemiolo, B., and Carmack, M. (1995) *Experientia 51*, 738−743.
25. North, M., and Pattenden, G. (1990) *Tetrahedron 46*, 8267−8290.
26. Riesenberg, D., Menzel, K., Schulz, V., Schumann, K., Veith, G., Zuber, G., and Knorre, W. A. (1990) *Appl. Microbiol. Biotechnol. 34*, 77−82.
27. Bax, A., and Subramanian, S. (1986) *J. Magn. Reson. 67*, 565−569.
28. Wishart, D. S., Bigam, C. G., Yao, J., Abildgaard, F., Dyson, H. J., Oldfield, E., Markley J. L., and Sykes, B. D. (1995) *J. Biomol. NMR 6*, 135−140.
29. Kay, L. E., Keifer, P., and Saarinen, T. (1992) *J. Am. Chem. Soc. 114*, 10663−10665.
30. Cavanagh, J., Fairbrother, W. J., Palmer, A. G., III, and Skelton, N. J. (1996) *Protein NMR Spectroscopy. Principles and Practice*, pp 419−422, Academic Press, New York.
31. Zhang, O., Kay, L. E., Olivier, J. P., and Forman-Kay, J. D. (1994) *J. Biomol. NMR 4*, 845−858.
32. Kuboniwa, H., Grzesiek, S., Delaglio, F., and Bax, A. (1994) *J. Biomol. NMR 4*, 871−878.
33. Vuister, G. W., and Bax, A. (1993) *J. Am. Chem. Soc. 115*, 7772−7777.
34. Kay, L. E., Nicholson, L. K., Delaglio, F., Bax, A., and Torchia, D. A. (1992) *J. Magn. Reson. 97*, 359−375.
35. Muhandiram, D. R., and Kay, L. E. (1994) *J. Magn. Reson., Ser. B 103*, 203−216.
36. Bax, A., and Ikura, M. (1991) *J. Biomol. NMR 1*, 99−104.
37. Yamazaki, T., Lee, W., Arrowsmith, C. H., Muhandiram, D. R., and Kay, L. E. (1994) *J. Am. Chem. Soc. 116*, 11655−11666.
38. Yamazaki, T., Lee, W., Revington, M., Mattiello, D. L., Dahlquist, F. W., Arrowsmith, C. H., and Kay, L. E. (1994) *J. Am. Chem. Soc. 116*, 6464−6465.

39. Kay, L. E., Xu, G.-Y., Singer, A. U., Muhandiram, D. R., and Forman-Kay, J. D. (1993) *J. Magn. Reson., Ser. B 101*, 333−337.
40. Yamazaki, T., Forman-Kay, J. D., and Kay, L. E. (1993) *J. Am. Chem. Soc. 115*, 11054−11055.
41. Zwahlen, C., Legault, P., Vincent, S. J. F., Greenblatt, J., Konrat, R., and Kay, L. E. (1997) *J. Am. Chem. Soc. 119*, 6711−6721.
42. Marion, D., Ikura, M., Tschudin, R., and Bax, A. (1989) *J. Magn. Reson. 85*, 393−399.
43. States, D. J., Haberkorn, R., and Ruben, D. J. (1982) *J. Magn. Reson. 48*, 286−292.
44. Wishart, D. S., Sykes, B. D., and Richards, F. M. (1992) *Biochemistry 31*, 1647−1651.
45. Wishart, D. S., and Sykes, B. D. (1994) *J. Biomol. NMR 4*, 171−180.
46. Chen, Y., Reizer, J., Saier, M. H., Fairbrother, W. J., and Wright, P. E. (1993) *Biochemistry 32*, 32−37.
47. Feeney, J., and Birdsall, B. (1993) in *NMR of Macromolecules. A Practical Approach* (Roberts, G. C. K., Ed.) p 187, Oxford University Press, Oxford, U.K.

BI990497T